Nb-based MXenes for Li-ion battery applications

Nb-based MXenes for Li-Ion Battery Applications

Jiajie Zhu[1], Alexander Chroneos[2,3,a] and Udo Schwingenschlögl[1,b]

[1]PSE Division, KAUST, Thuwal 23955-6900, Kingdom of Saudi Arabia

[2]Department of Materials, Imperial College, London SW7 2AZ, United Kingdom

[3]Faculty of Engineering and Computing, Coventry University, Priory Street,

Coventry CV1 5FB, United Kingdom

[a]Email: alexander.chroneos@imperial.ac.uk

[b]Email: udo.schwingenschlogl@kaust.edu.sa

October 29, 2015

Abstract

Li-ion batteries depend critically on the stability and capacity of the electrodes. In this respect the recently synthesized two-dimensional MXenes are promising materials, as they combine an excellent Li-ion capacity with very high charging rates. We employ density functional theory to investigate the impact of Li adsorption on the structural and electronic properties of monolayer Nb_2C and Nb_2CX_2. The Li ions are predicted to migrate easily on the pristine MXene due to a diffusion barrier of only 36 meV, whereas larger diffusion barriers are obtained for the functionalized MXenes.

Keywords: Nb_2C, MXene, Battery

1 Introduction

Besides graphene, the quickly growing family of two-dimensional materials includes boron nitride,[1] transition metal chalcogenides,[2] and metal oxides,[3] for example, and recently also the socalled MXenes.[4–7] MXenes are early transition metal carbides and/or carbonitrides[8] that can be prepared by selective etching of the A metal from the three-dimensional $M_{n+1}AX_n$ phases (n: integer, M: early transition metal, A: group 13-16 element, and X: C and/or N). They have hexagonal symmetry (space group P63/mmc) and are typically characterized by a combination of both ceramic (high decomposition or melting temperature, high elastic stiffness, and good machinability) and metallic (high thermal shock resistance and good thermal and electrical conductivities) features, resulting from the stacking of n "ceramic" MX layer(s) separated by the "metallic" A layer.

There are many potential applications for MXenes, for example in catalysts, sensors, conductive reinforcement fillers for polymers, electronic and optoelectronic devices, and electrodes of supercapacitors for electrical energy storage.[9–14] Importantly, MXenes have been identified as candidate materials for Li-ion batteries. For example, the Li storage capacity of Ti_3C_2 is comparable with commercial graphite electrodes (372 mAh/g).[15] In addition, a small Li diffusion barrier enables high cycling rates and most metallic MXenes show a higher electrical conductivity than other two-dimensional materials.[16]

Although many MXenes have been synthesized, including Ti_2C, $(Ti_{0.5}Nb_{0.5})_2C$, Ti_3C_2, Ti_3CN, Ta_4C_3, Nb_2C, V_2C, and $(V_{0.5}Cr_{0.5})_3C_2$,[4,17] only the titanium carbides have been investigated intensively to obtain insight into the excellent material performance.[15,18–21] For V_2C a much higher capacity of 941 mAh/g as compared to the experimental value of 260 mAh/g has been predicted theoretically.[22] As compared to the widely studied M_3X_2-type compound, M_2X-type compound can store more Li per gram (thus having a higher capacity) because the surface-to-volume ratio is larger. While a high capacity combined with a high cycling rate has been reported also for Nb_2C,[17] this material has received little attention so far. Therefore, we present in the following theoretical insight into the applicability of Nb_2C in Li-ion batteries. Because Nb_2C can be functionalized by O, F, and OH due to the presence of HF and H_2O during the preparation,[23] we consider the effects of these functional groups on the Li adsorption.

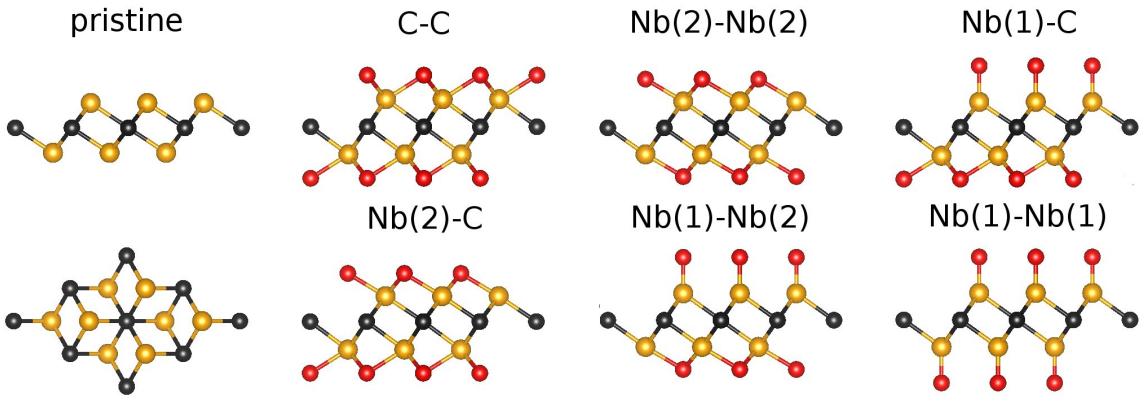

Figure 1: Structures of Nb_2C (side and top views) and Nb_2CX_2 (top views) for different locations of the functional group (red). The Nb and C atoms are shown in yellow and black color.

2 Computational method

Our theoretical framework is density functional theory, using the projector augmented wave method of the Vienna Ab-initio Simulation Package.[24] The generalized gradient approximation of Perdew, Burke and Ernzerhof is employed for the exchange-correlation potential and the long range van der Waals interaction is taken into account by the DFT-D3 approach[25] (which is not critical for the following evaluations, since the relevant properties are determined by much stronger chemical interactions). The cut-off energy for the plane wave basis functions is set to 500 eV and an energy criterion of 10^{-6} eV is selected in the iterative solution of the Kohn-Sham equations. All the structures are relaxed until the residual forces on the atoms have declined to less than 0.01 eV/Å. Brillouin zone integrations are performed on $6 \times 6 \times 1$ and $12 \times 12 \times 1$ k-meshes, respectively, for the geometry optimization and electronic structure calculations. A 2×2 supercell of monolayer Nb_2C is used together with a vacuum layer of 15 Å thickness to avoid unphysical interaction between images due to the periodic boundary conditions. A climbing image nudged elastic band method is employed to investigate the energy barriers of Li diffusion, with 7 to 9 images between the initial and final configurations, and to calculate the minimum energy migration paths.[26]

3 Results and discussion

Figure 1 shows the structures of Nb_2C and Nb_2CX_2. The X group can be located on top of a C atom, a Nb(1) atom (top Nb layer), and a Nb(2) atom (bottom Nb layer), on both sides of the

Table 1: Distance from the Nb(1) atom to the functional group, which is located on top of the C, Nb(1), or Nb(2) atoms.

	C	Nb(1)	Nb(2)
Nb-O	2.14 Å	1.72 Å	2.09 Å
Nb-F	2.28 Å	1.88 Å	2.29 Å
Nb-OH	2.25 Å	1.90 Å	2.27 Å

MXene. Thus a total of six configurations has to be considered. We will refer in the following to these configurations using the nomenclature defined in Figure 1. For Nb_2C the in-plane lattice constant turns out to be 3.086 Å, which agrees well with the experimental value of 3.107 Å[27] and other theoretical values,[28,29] and the Nb-C bond length to be 2.16 Å. Configuration Nb(2)-Nb(2) has the lowest total energy for all functional groups, confirming Ref. 30. We note that the Nb(1)-F and Nb(1)-OH bond lengths are similar and both larger than the Nb(1)-O bond length, reflecting the different oxidation states of the functional groups.

We find that the energetically favorable site for Li adsorption is located on top of C. The stability of this configuration is determined by the formation energy with respect to a reference material,

$$E = E_{\text{combined}} - E_{\text{MXene}} - E_{\text{reference}}, \tag{1}$$

where E_{combined}, E_{MXene}, and $E_{\text{reference}}$ are the total energies of the combined system in the lowest energy structure, the MXene without Li, and the reference material. For a single Li atom on Nb_2C and Nb_2CX_2 (X = O, F and OH) we obtain formation energies of -0.71, -2.28, -1.61, and 0.51 eV, respectively, with respect to bulk Li. The positive value for $Nb_2C(OH)_2$ reflects instability, in agreement with related theoretical results,[31] and points to the formation of Li clusters. The value for Nb_2CO_2 is significantly more negative than that for Nb_2CF_2, because the oxidation state of O is more negative than that of F. The stabilities of the O and F groups are investigated as LiF and Li_2O could be formed. Moreover, a 3:1 ratio of O and F functional groups will be addressed as it is motivated by the experiment.[17] The O group associated with two Li atoms results in formation energies of -2.47 and -2.53 eV for Nb_2CO_2 and $Nb_2CO_{1.5}F_{0.5}$, respectively, with respect to Li_2O, reflecting stability. Furthermore, we obtain for the F group associated with one Li atom values of 0.09 and -0.54 eV for Nb_2CF_2 and $Nb_2CO_{1.5}F_{0.5}$, respectively, with respect to LiF. The instability of the F group for Nb_2CF_2 agrees with results reported for V_2C and Ti_3C_2.[22,32] On the other hand, the strong interaction

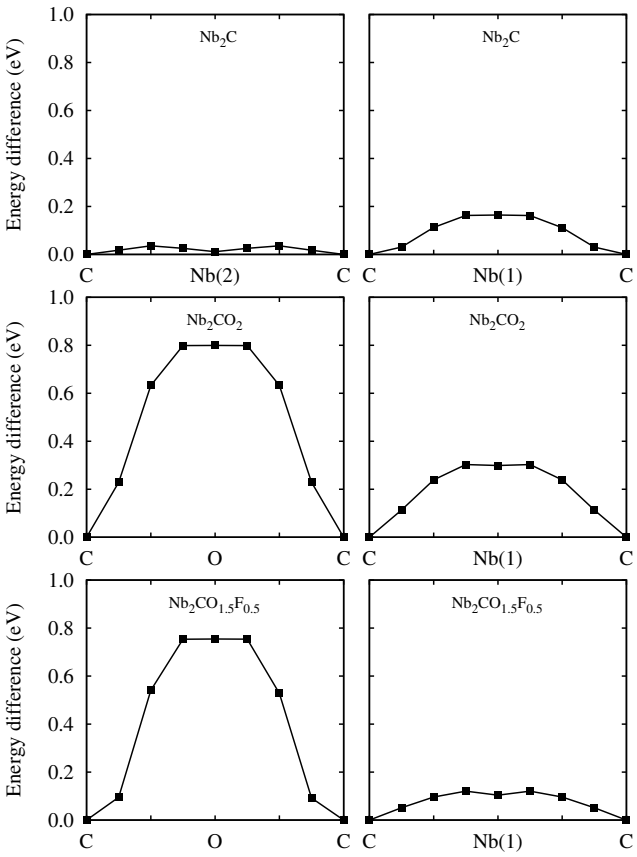

Figure 2: Diffusion barriers for Li on Nb_2C and Nb_2CX_2.

with neighbouring O atoms stabilizes the F group on $Nb_2CO_{1.5}F_{0.5}$. Due to the above results, the F and OH groups will not be considered in the following.

Diffusion barriers for Li migration are addressed in Figure 2, considering the three migration paths defined in Figure 3. All migration paths turn out to consist of almost straight segments. For Nb_2C path C-C converges to path C-Nb(2)/O-C and for Nb_2CO_2, Nb_2CF_2, and $Nb_2CO_{1.5}F_{0.5}$ path C-C converges to path C-Nb(1)-C. For Nb_2C path C-Nb(2)/O-C has the lowest diffusion barrier of 36 meV with the transition state located on top of the C-Nb(2) bond. A local minimum is located on top of the Nb(2) atom with 12 meV higher energy. The diffusion barrier along path C-Nb(1)-C amounts to 160 meV. In the cases of the functionalized MXenes path C-Nb(1)-C has the lowest diffusion barrier with values of 300 and 120 meV for Nb_2CO_2 and $Nb_2CO_{1.5}F_{0.5}$, respectively, while for path C-Nb(2)/O-C we obtain values of 800 and 750 meV. The transition state is located almost on top of the Nb(1) atom for Nb_2CO_2 and $Nb_2CO_{1.5}F_{0.5}$. Therefore, easy migration is achieved on Nb_2C, whereas all functional groups significantly increase the diffusion barriers. This fact can be understood in terms of the charge

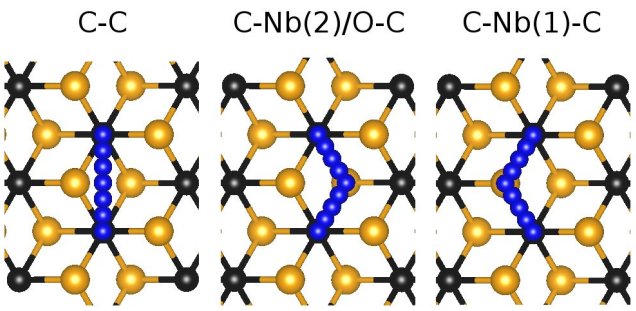

Figure 3: Migration paths under consideration. Note that paths C-Nb(2)/O-C and C-Nb(1)-C are not symmetric in the presence of functional groups, which are not shown in the figure.

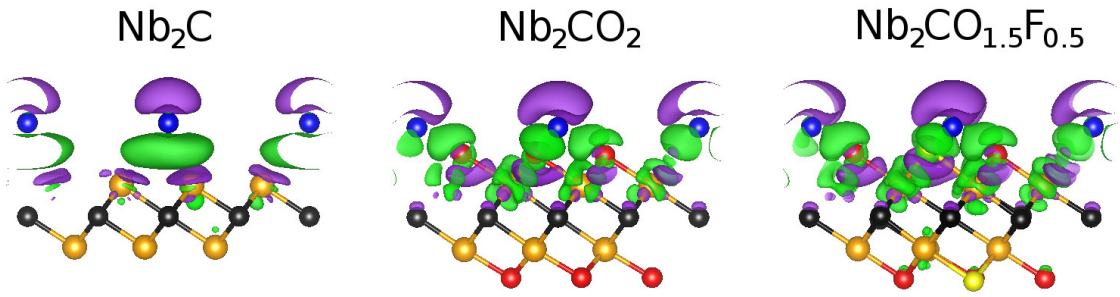

Figure 4: Ground state charge redistribution due to the interaction with Li. Green/purple color represents charge accumulation/depletion, where the isosurfaces refer to an isovalue of 1.8×10^{-3} electrons/bohr^3. The Nb, C, O, F, and Li atoms are shown in yellow, black, red, light yellow and blue color.

density differences due to the interaction with Li atoms,

$$\Delta\rho = \rho_{\text{combined}} - \rho_{\text{MXene}} - \rho_{\text{Li}}, \tag{2}$$

as illustrated in Figure 4. Here ρ_{combined}, ρ_{MXene}, and ρ_{Li} are the charge densities of the combined system, MXene, and Li atom, respectively. While there is no qualitative difference between the results for the functionalized MXenes, we observe a strongly reduced interaction for bare Nb_2C. This picture is supported by the densities of states shown in Figure 5. No Li $2s$ contributions are found below -2 eV for bare Nb_2C in contrast to the cases of the functionalized MXenes, again demonstrating weak interaction. We note that the metallic nature of Nb_2C and Nb_2CX_2 as shown in Figure 5 is highly desirable for application in Li-ion batteries.

In order to calculate the Li specific capacities of the different materials, we consider the maximal Li adsorption. Adsorption beyond a monolayer on both sides of the MXene is not addressed, since Li clusters are hard to decompose during the recharge process due to the large binding energy. We find that Nb_2C can adsorb up to 9 Li atoms per 2×2 supercell,

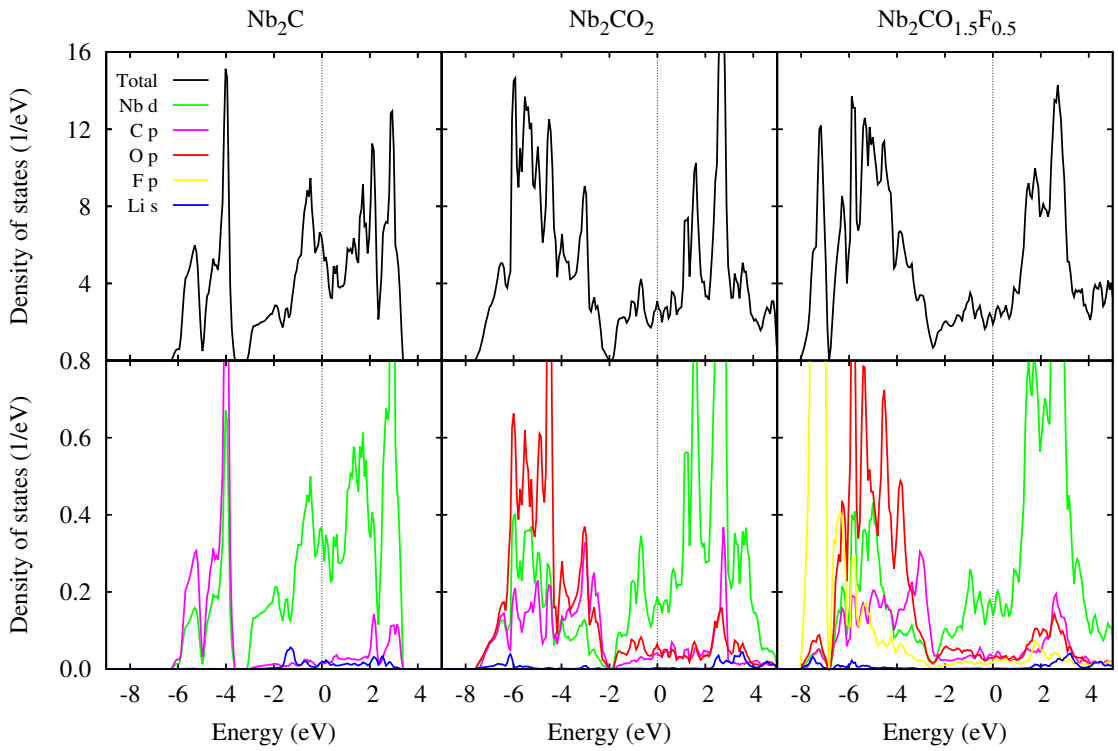

Figure 5: Densities of states after Li decoration. The Fermi level is set to zero.

8 located on top of or below C and the last one on top of Nb(2). This corresponds to a maximal Li concentration of 2.25 atoms per unit cell. Nb_2CO_2 can accommodate 10 Li atoms per 2×2 supercell, 6 on one side and 4 on the other side, which corresponds to a maximal Li concentration of 2.5 atoms per unit cell. In contrast to Nb_2C, here two Li ions are located on top of Nb(2) without forming a Li cluster (strong interaction with the MXene). Although the F group is stable on $Nb_2CO_{1.5}F_{0.5}$ with a Li atom attached, LiF will be formed when more Li atoms are adsorbed. $Nb_2CO_{1.5}F_{0.5}$ can accomodate only two Li atoms, one on each side.

We obtain specific capacities of 305 and 292 mAh/g for Nb_2C and Nb_2CO_2, whereas the corresponding value for the O/F system is only 29 mAh/g. Although F is inclined to react with Li to LiF, further Li atoms can be adsorbed. Hence, the experimental value of 170 mAh/g can be attributed to the mixture of O and F groups.[17] However, LiF obstructs the Li migration and thus leads to a degraded performance for high cycling rates. The calculated specific capacity is comparable to the high value of Ti_3C_2 (320 mAh/g).[32]

4 Conclusions

The structural and electronic properties of Li decorated Nb_2C and Nb_2CX_2 have been investigated by first principles calculations. The favorable adsorption sites of the functional groups have been determined. Since Li will form clusters on $Nb_2C(OH)_2$ and LiF on Nb_2CF_2 and $Nb_2CO_{1.5}F_{0.5}$, OH and F functional groups must be avoided in battery applications. We find the by far lowest diffusion barrier for Li on Nb_2C. Specific capacities of 305 and 292 mAh/g are obtained for Nb_2C and Nb_2CO_2, respectively. Since the diffusion barrier for Nb_2CO_2 is high, Nb_2C without functionalization turns out to be the most promising electrode material for Li-ion batteries.

Acknowledgment

Research reported in this publication was supported by the King Abdullah University of Science and Technology (KAUST).

References

[1] Novoselov, K. S.; Jiang, D.; Schedin, F.; Booth, T. J.; Khotkevich, V. V.; Morozov, S. V.; Geim, A. K. *Proc. Natl. Acad. Sci. U.S.A.* **2005**, *102*, 10451–10453.

[2] Jeong, S.; Yoo, D.; Jang, J.-T.; Kim, M.; Cheon, J. *J. Am. Chem. Soc.* **2012**, *134*, 18233–18236.

[3] Ma, R.; Sasaki, T. *Adv. Mater.* **2010**, *22*, 5082–5104.

[4] Eames, C.; Islam, M. S. *J. Am. Chem. Soc.* **2014**, *136*, 16270–16276.

[5] Lei, J.-C.; Zhang, X.; Zhou, Z. *Front. Phys.* **2015**, *10*, 276–286.

[6] Zhang, X.; Ma, Z.; Zhao, X.; Tang, Q.; Zhou, Z. *J. Mater. Chem. A* **2015**, *3*, 4960–4966.

[7] Tang, Q.; Zhou, Z. *Prog. Mater. Sci.* **2013**, *58*, 1244–1315.

[8] Naguib, M.; Mochalin, V. N.; Barsoum, M. W.; Gogotsi, Y. *Adv. Mater.* **2014**, *26*, 992–1005.

[9] Zhang, X.; Xu, J.; Wang, H.; Zhang, J.; Yan, H.; Pan, B.; Zhou, J.; Xie, Y. *Angew. Chem. Int. Ed.* **2013**, *52*, 4361–4365.

[10] Hu, Q.; Sun, D.; Wu, Q.; Wang, H.; Wang, L.; Liu, B.; Zhou, A.; He, J. *J. Phys. Chem. A* **2013**, *117*, 14253–14260.

[11] Wang, F.; Yang, C.; Duan, C.; Xiao, D.; Tang, Y.; Zhu, J. *J. Electrochem. Soc.* **2015**, *162*, B16–B21.

[12] Lee, Y.; Hwang, Y.; Cho, S. B.; Chung, Y.-C. *Phys. Chem. Chem. Phys.* **2014**, *16*, 26273–26278.

[13] Ma, Z.; Hu, Z.; Zhao, X.; Tang, Q.; Wu, D.; Zhou, Z.; Zhang, L. *J. Phys. Chem. C* **2014**, *118*, 5593–5599.

[14] Gao, Y.; Wang, L.; Li, Z.; Zhou, A.; Hu, Q.; Cao, X. *Solid State Sci.* **2014**, *35*, 62–65.

[15] Er, D.; Li, J.; Naguib, M.; Gogotsi, Y.; Shenoy, V. B. *ACS Appl. Mater. Inter.* **2014**, *6*, 11173–11179.

[16] Lee, Y.; Cho, S. B.; Chung, Y.-C. *ACS Appl. Mater. Inter.* **2014**, *6*, 14724–14728.

[17] Naguib, M.; Halim, J.; Lu, J.; Cook, K. M.; Hultman, L.; Gogotsi, Y.; Barsoum, M. W. *J. Am. Chem. Soc.* **2013**, *135*, 15966–15969.

[18] Xie, Y.; Kent, P. R. C. *Phys. Rev. B* **2013**, *87*, 235441.

[19] Enyashin, A.; Ivanovskii, A. *J. Solid State Chem.* **2013**, *207*, 42–48.

[20] Zhao, S.; Kang, W.; Xue, J. *J. Phys. Chem. C* **2014**, *118*, 14983–14990.

[21] Sun, D.; Wang, M.; Li, Z.; Fan, G.; Fan, L.-Z.; Zhou, A. *Electrochem. Commun.* **2014**, *47*, 80–83.

[22] Hu, J.; Xu, B.; Ouyang, C.; Yang, S. A.; Yao, Y. *J. Phys. Chem. C* **2014**, *118*, 24274–24281.

[23] Li, Z.; Wang, L.; Sun, D.; Zhang, Y.; Liu, B.; Hu, Q.; Zhou, A. *Mater. Sci. Eng. B* **2015**, *191*, 33–40.

[24] Kresse, G.; Joubert, D. *Phys. Rev. B* **1999**, *59*, 1758–1775.

[25] Grimme, S.; Antony, J.; Ehrlich, S.; Krieg, H. *J. Chem. Phys.* **2010**, *132*, 154104.

[26] Henkelman, G.; Uberuaga, B. P.; Jnsson, H. *J. Chem. Phys.* **2000**, *113*, 9901–9904.

[27] Salama, I.; El-Raghy, T.; Barsoum, M. *J. Alloy. and Compd.* **2002**, *347*, 271–278.

[28] Wang, J.; Zhou, Y. *Phys. Rev. B* **2004**, *69*, 214111.

[29] Qian, X.; Li, Y.; He, X.; Fan, H.; Yun, S. *J. Phys. Chem. Solids* **2011**, *72*, 954–956.

[30] Khazaei, M.; Arai, M.; Sasaki, T.; Chung, C.-Y.; Venkataramanan, N. S.; Estili, M.; Sakka, Y.; Kawazoe, Y. *Adv. Funct. Mater.* **2013**, *23*, 2185–2192.

[31] Xie, Y.; DallAgnese, Y.; Naguib, M.; Gogotsi, Y.; Barsoum, M. W.; Zhuang, H. L.; Kent, P. R. C. *ACS Nano* **2014**, *8*, 9606–9615.

[32] Tang, Q.; Zhou, Z.; Shen, P. *J. Am. Chem. Soc.* **2012**, *134*, 16909–16916.